Applied Physics A (2020) 126:960
https://doi.org/10.1007/s00339-020-04067-3

Applied Physics A
Materials Science & Processing

An effect of precursor concentrations on the photodetection capabilities of CdS thin films for high-efficiency visible-light photodetector applications

M. Dharani Devi[1] · A. Vimala Juliet[1] · K. Hari Prasad[2] · T. Alshahrani[3] · A. M. Alshehri[4] · Mohd. Shkir[4] · S. AlFaify[4]

Received: 28 July 2020 / Accepted: 12 October 2020 / Published online: 2 December 2020

Abstract
Photo-conducting CdS films were coated on glass at 450 °C using cadmium chloride and thiourea as Cd and S sources, respectively, with different concentrations. The sprayed CdS films are crystallized in the hexagonal structure and orienting along (0 0 2) plane with good adherence. All the films have high optical absorption in the visible region showing optical bandgap values in the range of 2.39–2.43 eV. The variation of precursor alters the surface morphology of the films. The formed grains are uniformly spread over the substrate and highly agglomerated at 0.15 M concentration. Band to band emission and defect-related emission are reported using photoluminescence (PL) measurements. The CdS device shows relatively high photosensitivity of 0.4 A/W, detectivity of 8.46×10^{10} Jones, external quantum efficiency (EQE of 140%) with a rise time about 0.2 s and decay time about 0.3 s. These results propose that the CdS thin films are potential candidates for the visible photo-detector applications prepared using an easy and low-cost fabrication method.

Keywords CdS thin films · Molar concentration · Direct bandgap · Photosensitivity · Photodetector

1 Introduction

The development of photodetectors towards photodetection usages based on advanced semiconducting materials is in the marvellous demand of optoelectronic industries for device fabrication [1–12]. They are also exploited for space, photonics, communications, etc. applications. Among these, the photodetectors based on cadmium sulfide (CdS) are noticed to be of current interest for the development of CdS-based photodetector with high detectivity, responsivity and quantum efficiency [13–20]. Also, CdS has been used to make heterostructures with ZnO/ZnS/P3HT, etc. for UV/visible photodetection [21–23]. Still, there is a great requirement of photodetectors with quick response and high-speed operations. CdS possess direct energy gap, and it has several other key applications as FETs, sensor/PEC sensor, energy/photovoltaics, etc. [16, 24–28]. The documented literature signifies that the electrical nature of CdS is remarkably improved when tested under some light [29]. Several methodologies have been developed and implemented to fabricate pure & doped CdS film-based photodetectors. Jie et al. prepared CdS single-crystallite nanoribbon-based photodetectors by CVD and noticed a significant increase in photoresponse compared to bulk CdS [20]. Bhushan et al. fabricated CdS/Nd/Pr@CdS by dipping route and studied photoconduction nature [29]. Mehdi et al. fabricated the CdS photodetector through the thermal process and showed high response-sensitivity/quantum efficiency of 0.82×10^3 A/W/0.66×10^3 to 1.8×10^3% [19, 30]. Wu et al. prepared the Ga@CdS/Au-based photodetector via thermal evaporation with rise/decay times of 95/290 µs [13, 31]. Dai et al. fabricated CdS NB-based MESFETs via CVD with high responsivity (~ 2.0×10^2 A/W) and quantum efficiency (~ 5.2×10^2) and rise/decay time of 137/379 µs [16]. Husham et al. and Waldiya et al. documented the CdS photodetectors

✉ A. Vimala Juliet
hod.eie.ktr@srmist.edu.in

[1] Department of EIE, SRM Institute of Science and Technology, Kattatankullathur, Chennai 603203, India

[2] Department of Physics, Institute of Aeronautical Engineering, Dundigal, Hyderabad 500043, India

[3] Department of Physics, College of Science, Princess Nourah Bint Abdulrahman University, Riyadh 11671, Saudi Arabia

[4] Advanced Functional Materials and Optoelectronics Laboratory (AFMOL), Department of Physics, Faculty of Science, King Khalid University, Abha 61413, Saudi Arabia

fabrication via the CBD process [32, 33]. Munde et al. casted CdS film-based photodetector via spray route [34]. Recently, Shkir et al. also fabricated the high-performance photodetectors based on Pr/Sm/Eu doped CdS films via spray pyrolysis route [35–37]. There are many other reports too on pure/doped CdS films/nanostructures preparation through different routes with modified properties [12, 16, 30, 38–45]. As per the above-cited reports, it is noticed that several routes are employed to fabricate CdS film-based photodetectors. Among them, spray pyrolysis is a relatively low-cost and facile one. Parameshwari et al. reported the spray pyrolysis fabrication of CdS by taking different molarities of Cd/S ($CdCl_2$/NH_2CSNH_2) and investigated for structure–morphology–optical and electrical properties [46].

However, varying molarity-based (Cd/S from $CdCl_2$/thiourea) fabrication of CdS photodetectors via optimized spray pyrolysis routes are not documented so far. Hence, we have casted CdS films via the nabulizer spray pyrolysis (NSP) route by taking both Cd and S precursors in 0.05, 0.10, and 0.15 M on the hot substrate at 450 °C for photodetection applications. The grown films were tested for phase approval via X-ray diffraction (XRD), morphology via scanning electron microscopy (SEM), the elemental composition by energy-dispersive X-ray spectroscopy (EDXS), optical bandgap evaluation via photoluminescence/UV–Vis spectroscopy and finally photodetectors were fabricated, and inspected their responsivity (R), detectivity (D^*), and efficiency (EQE) under 532 nm laser source.

2 Experimental procedure

2.1 Materials and preparation

Thin CdS films were coated on glass using a nebulizer spray pyrolysis technique. Different Cd:S molar ratio solution with an air of pressure of 1.5 kg/cm^2 as a carrier gas. The deposition temperature was set to 450 °C. Prior to the casting of films, the substrates were immersed in chromic acid for 30 min and cleaned with water via an ultrasonic bath. Sprayed the mixed $CdCl_2$ and thiourea precursors solution of different molarities (0.05, 0.10, and 0.15 M) was as 1 ml/min. Preserved a 5-cm spacing was among nozzle and substrate.

2.2 Measurements

The crystal structure of the coated CdS films was investigated via an X-ray diffractometer (XRD) using CuKα radiation in the 2θ values in the range of 10°–80°. The morphology was inspected via ZEISS-EVO 18 SEM. PL Spectrometer (Perkin Elmer Model: LS 45) (With excitation wavelength λ_{exc} = 450 nm) was employed to collect emission profiles. The absorption profiles of the film were recorded via Perkin Elmer: Lambda 35. Stylus profilometer was used to measure the thickness of films as listed in Table 1. For photoconductivity measurements, the silver paste with 2 mm dia. was used as electrodes on top surfaces of CdS films to fabricate MSM visible photodetector. The size of the film and area of irradiation was 0.1 × 0.2 cm and ~ 0.02 cm^2, correspondingly. All the photoconductivity measurements were measured at room temperature using a Keithley (Model-2450) under 532 nm laser irradiation.

Table 1 Film thickness and structural parameters of prepared CdS thin films

Molarity (M)	Film thickness (nm)	Crystallite size (nm)	Strain ($\times 10^{-3}$)
0.05	450	54	0.743
0.10	500	74	0.593
0.15	470	71	0.687

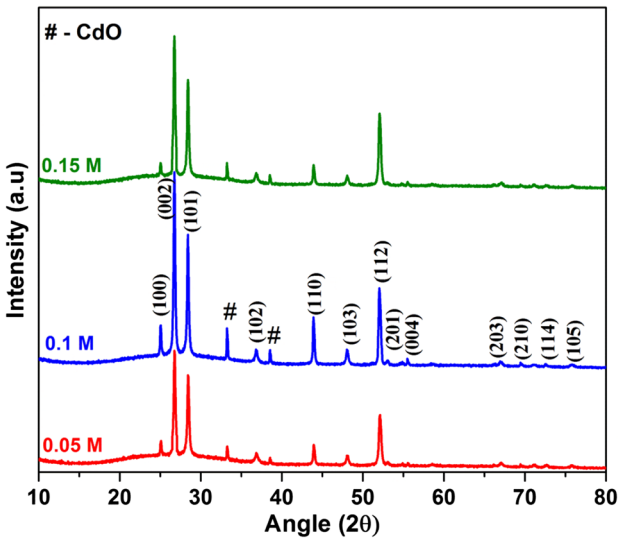

Fig. 1 X-ray diffraction patterns of CdS thin films at different molar concentrations

3 Results and discussion

3.1 XRD analysis

XRD is a favorable route to examine the phase of the fabricated CdS specimens. The obtained XRD patterns of the films are pictured in Fig. 1. The coated products on glass substrates exhibit three strong and ten weak Bragg reflections corresponding to (100), (002), (101), (102), (110), (103), (112), (201), (004), (203), (210), (114), and (105)

orientations, respectively. These observed patterns show that the prepared samples have a hexagonal structure of standard CdS with SG P63mc correlating to JCPDS # 41-1049 [47]. This hexagonal phase of CdS is stable and well suitable for device applications [48]. Moreover, the peak (002) is stronger than other labelled peaks indicating preferential growth orientation. A similar finding of CdS work is reported by Ravichandran et al. [49]. When molar concentration raised to 0.1 M, the sharpness of all the peaks systematically enhanced and later it is decreased for higher concentration which implies the degradation in the crystallinity [32]. Besides that, two additional impurity peaks of the CdO phase was also appeared. Recently Gosavi et al. [50] and Abdol Ahzadeh Ziabari et al. [51] recorded a similar kind of CdO phase in CdS and the presence of CdO phase may be due to higher coating temperature.

Williamson–Hall (W–H) method is a possible route to compute other structural characteristics like crystallite size (D) and lattice strain [52]:

$$\beta_{hkl}\cos\theta = \left(\frac{k\lambda}{D}\right) + (4\varepsilon\sin\theta). \quad (1)$$

A plot among $4\sin\theta$ and $\beta_{hkl}\cos\theta$ is drawn, in which y-intercept yields the D value and slope gives strain value. Figure 2a–c represents an enlarged view of the plotted graph concerning to molar concentration. The crystallite size and strain values deduced from the graph are presented in Table 1. It has been noticed that the D values are upraised from 54 to 74 nm and reduced to 71 nm for higher molar concentration. Anitha et al. observed similar crystallite size variation for nebulizer coated thin films [53]. The film prepared with 0.10 M appeared with a low strain value of 0.593×10^{-3} which ensures the quality of the specimens.

3.2 SEM analysis

SEM images were undertaken to demonstrate the surface homogeneity, size, film uniformity, and shape of the particles in films. Figure 3a–c depicts the captured surface microstructure images of CdS thin films at a fixed magnification. From these images, we confirm that the molar concentration notably changes the surface morphology of the products. In the first case, morphology appeared with very finely grown particles without distinguishable grain boundaries. However, it is changed when molar concentration is increased to 0.10 M. Observed the round-shaped particles with enlarged size on the top surface due to the mobilization of more particles with greater energy. And also, the unequally distributed crystallites might have been caused by van der Wall's forces [54]. The enhancement in the grain size as a function of molar concentration is as follows. When molar concentration is significantly less, the interaction between the substrate and CdS samples will

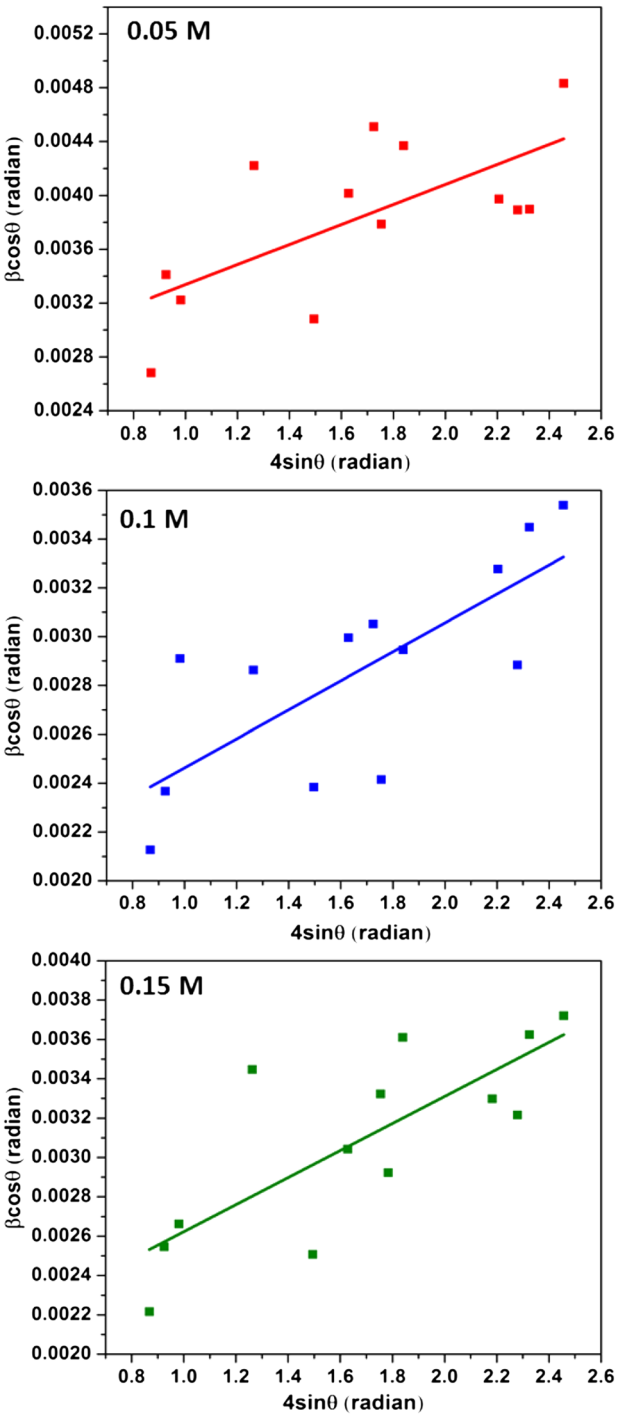

Fig. 2 Plot of $\beta\cos\theta$ vs $4\sin\theta$ of CdS thin films at different molar concentrations

be high, which resists the movement of the atoms and also it will stop the growth of the grain. Further, when molar concentration is raised, the average grain size becomes elongated due to nucleation occurrence [55]. Interestingly, porous nature is also observed in the 0.10 M coated sample. This porous structure morphology will improve the

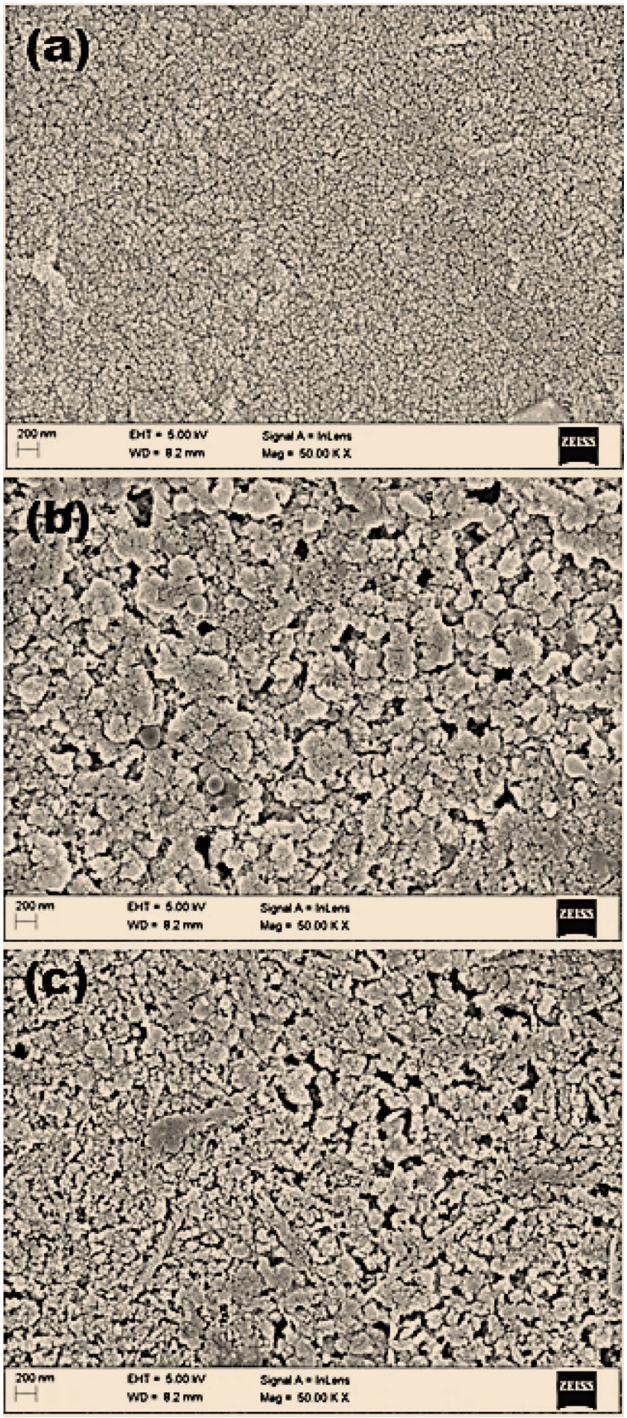

Fig. 3 SEM images of CdS thin films at different molar concentrations **a** 0.05 M, **b** 0.10 M and **c** 0.15 M

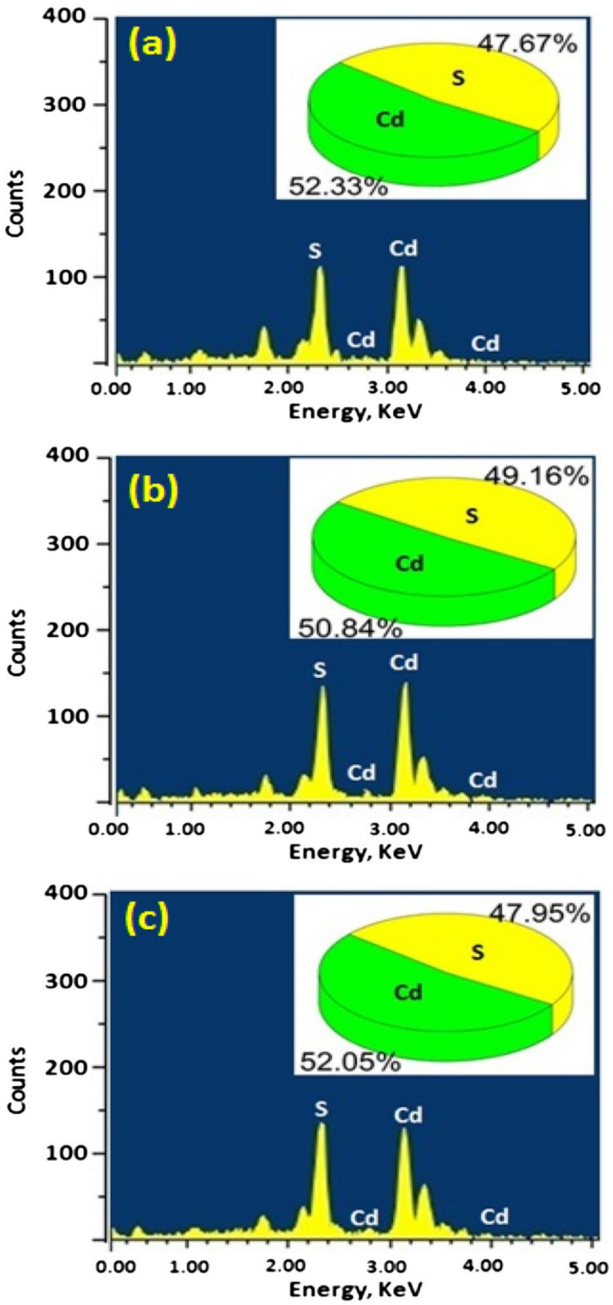

Fig. 4 EDX patterns of CdS thin films at different molar concentrations **a** 0.05 M, **b** 0.10 M and **c** 0.15 M

surface to volume ratio, which leads to light absorption efficiency. This system at upraised absorption behavior enhances electron–hole pairs generation, which leads to triggering its performance of photodetector [56]. In the last case (0.15 M), the grain size is small compared to the last one. These results perfectly matched with our XRD results. These interesting results are consistent with the earlier report of Husham et al. [57].

The elemental analysis of the CdS samples was done to ensure the chemical composition present in the coated products. Figure 4 presents the enlarged view of EDX patterns for 3-different molar contents 0.05, 0.10, and 0.15 M respectively. Peaks related to Cd and S confirm the presence of cadmium and sulfur with the stoichiometric ratio for the film prepared at 0.10 M concentration.

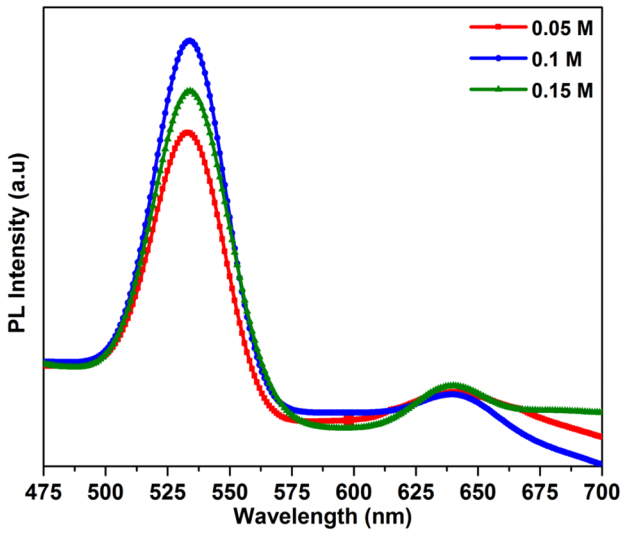

Fig. 5 PL spectra of CdS thin films at different molar concentrations

3.3 Photoluminescence analysis

PL spectroscopy study is an effective way to obtain valuable information about photoactive centers. Figure 5 shows the room temperature PL profiles of the CdS samples. As we visualize, all the CdS spectra reveal two luminescent centers observed at 532 nm and 638 nm. The predominant peak located at 532 nm is associated with band edge emission which might be due to the recombination of free excitons [37]. The peak positioned at 635 nm (broad) is occurred due to the surface-related defects [58]. Nupur Saxena and his lab mates mentioned that the green emission peak (532 nm) appeared in the CdS samples is assigned to the transition of S-vacancy and S-interstitial. The red emission peak (635 nm) is attributed to the transition of bound electrons from surface states to the valence band (VB) [59]. Moreover, the intensity and sharpness of the peak seem to enhance with increasing molar concentration up to 0.1 M, which indicates the high crystallinity of the CdS sample. When concentration is further raised, the intensity is decreased but not smaller than the 0.05 M coated sample. While upraising concentration, a slight red shift behavior is also observed due to increment in crystallite size [60].

3.4 UV–Vis absorption analysis

A detailed study on optical characteristics like absorption and bandgap of the CdS thin films was done via UV–Vis spectroscopy. Figure 6a, b elaborates the optical absorption spectra and Tauc's plots of the thin films grown on glass substrates with various molar concentrations. An abrupt increase in light absorption is noticed in the visible region as the molar concentration rises to 0.10 M, while for the film

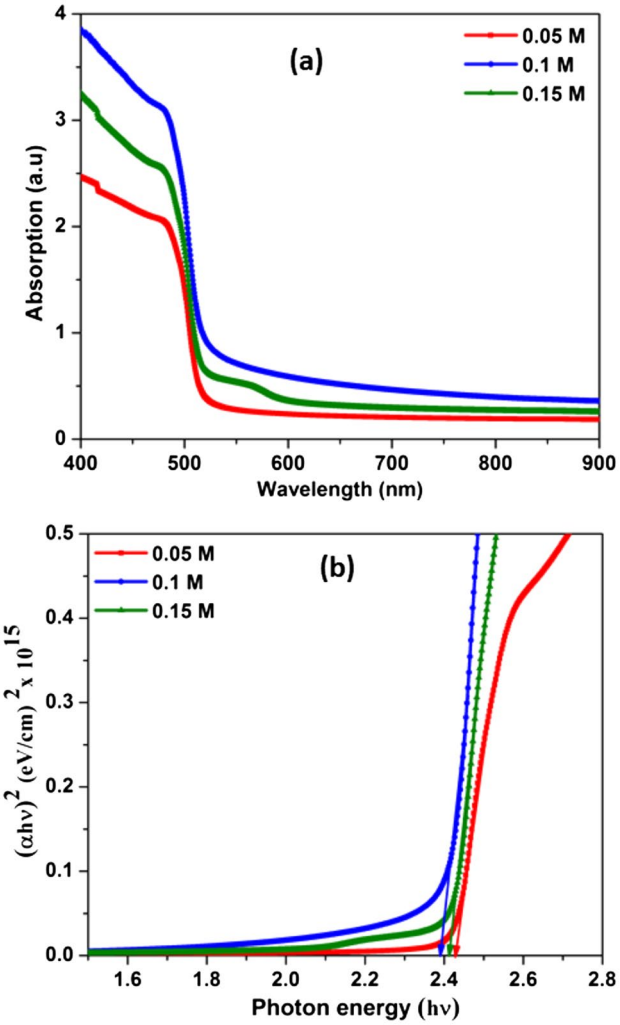

Fig. 6 **a** Absorption spectra as a function of wavelength and **b** a plot of $(\alpha h\nu)^2$ versus $(h\nu)$ of CdS thin films at different molar concentrations

grown with 0.15 M concentration, it is slightly reduced. In the case of the 0.10 M sample, the absorption level is high, so it can absorb more photons which can increase photosensing activity in the synthesized product [61]. On the other side, the fundamental edge of absorption was moved to a larger wavelength zone on the rise of concentration suggesting a bandgap lessening. This shifting nature may be due to the variation of grain size [55]. Nair and his lab mate obtained similar results [62]. Another crucial optical parameter, i.e. bandgap energy (Eg) of the samples, was computed trough Tauc's relation [63]:

$$\alpha h\nu = B(h\nu - E_g)^n .$$

Here, α denotes the coefficient of absorption and B is constant. The E_g value of the sample coated with 0.05 M

concentration is found to be 2.43 eV, and it is decreased to 2.39 eV for a 0.10 M coated sample. On the other side, it is raised to 2.41 eV for the last sample prepared with 0.15 M. Parameshwari et al. reported similar kinds of bandgap variation with respect to molar concentration for CdS films manufactured via spray process [46]. Few parameters such as crystallite size, lattice strain and point defects can reduce the energy gap value. In our present samples, the lowest E_g value may be due to a change in crystallite size variation.

3.5 Photodetector analysis

We investigated the photodetection properties of the manufactured CdS thin films as a function of molar variation. Figure 7a publicizes the schematic illustration of the deposited samples. In this study, we measured the *I–V* features of products with and without 532 nm laser light using Keithley 2450 source meter. Figure 7b–d illustrates the *I–V* plots of CdS films between − 5 and + 5 V. From the displayed figure, it can be seen that when the applied voltage is increased photocurrent of CdS films significantly increases for both dark and light conditions. The CdS films achieved with 0.1 M concentration exhibit a maximum net current of 2.5 µA and when the CdS samples are illuminated under the light with intensity 5 mW/cm^2, they absorb this light and create more electron–hole pairs, which are dissociating into electron and holes through samples built-in potential. Both of these are composed of electrodes and hence produced the photocurrent. Due to the following reasons, our CdS thin film coated with 0.1 M concentration exhibits the enhancement of illumination current: (i) high crystalline nature, (ii) large grain size value, (iii)

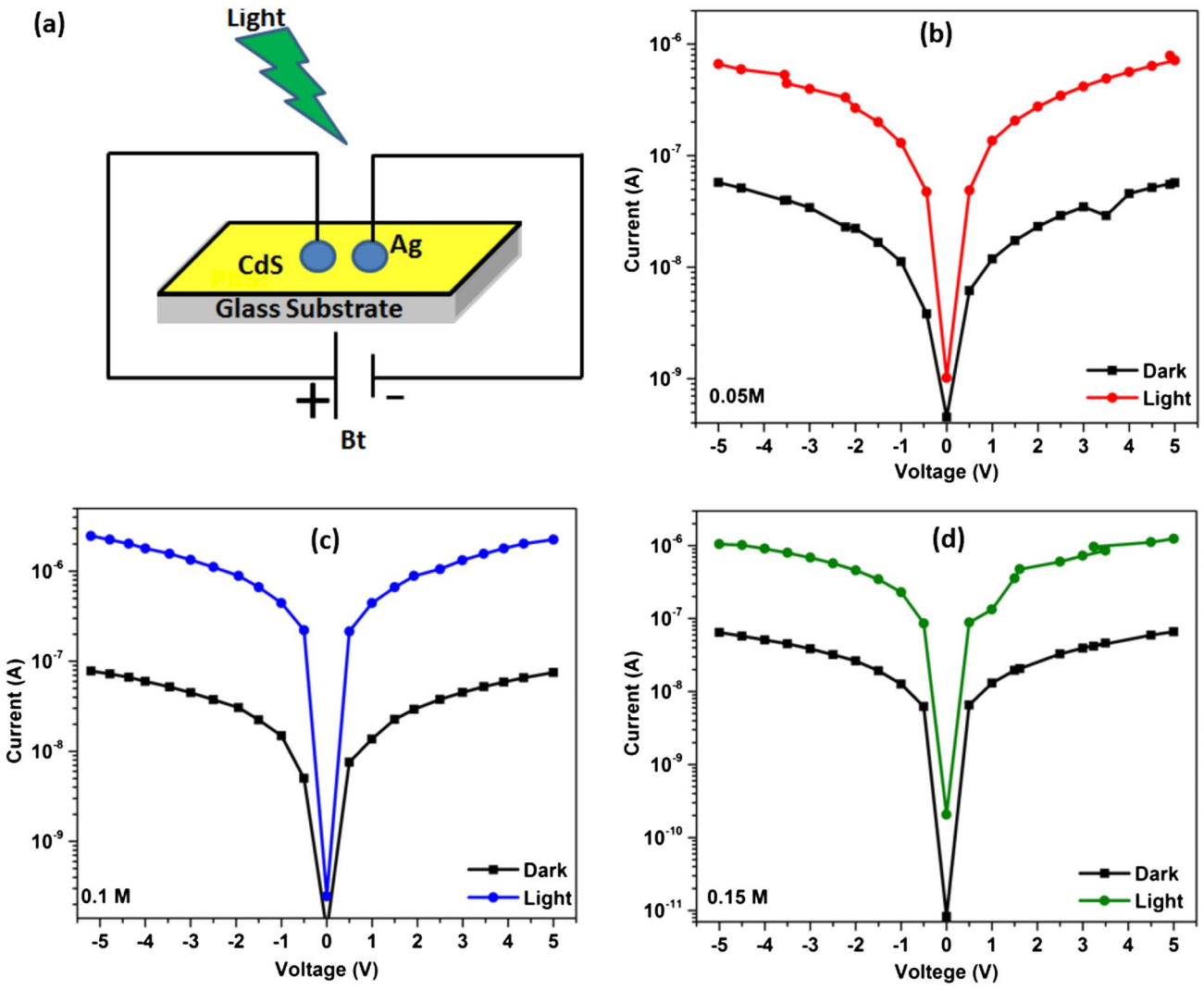

Fig. 7 **a** Schematic diagram CdS photosensor, Semi-log IV characteristics of the fabricated CdS photo sensor measured in dark and illumination condition at bias voltage between − 5 and 5 V prepared at **b** 0.05 M, **c** 0.10 M, and **d** 0.15 M

porous nature in the morphology, (iv) high absorption, and (v) lesser bandgap energy.

The calculation of three parameters like R, D^*, & EQE is essential because they generally indicate the performance of the photodetector. The following relation was used to calculate responsivity (R) easily [36] and Table 2 provides the respective values.

$$R = \frac{I_p}{P_{in} \times A}, \tag{3}$$

where I_p, A, and P are known as photocurrent, effective area, and light intensity.

The estimated responsivity of the CdS films is found to be 0.15, 0.43 and 0.24 A/W, respectively. Mohammed Husham and his co-workers [64] reported that prepared CdS material had the responsivity of 0.24 A/W. Manmohan Singh Waldiya and his lab mates [33] reported responsivity between 0.0715 and 0.3815 A/W. Thick CdS film prepared by Shivaji Munde et al. [34] exhibited a responsivity of 2.5 A/W. Compared to the above-reported values our samples show better responsivity of 0.43 A/W for 0.1 M concentration. The D^* was estimated by the below equation [36] and provided in Table 2:

$$D* = \sqrt{\frac{A}{2eI_{dark}}}, \tag{4}$$

where e and I_d are electron charge in dark current. The CdS thin film deposited with 0.05 M shows the specific detectivity of 3.48×10^{10} Jones. While raising molar concentration it goes up to 8.46×10^{10} Jones, then decreases to 5.10×10^{10} Jones for higher concentration. Compared to our current D value, Manlin Tan et al. [65] stated a value of 1.5×10^{12} Jones and Shkir et al. [35] reported a value of 6.94×10^{11} Jones which is higher. We also measured external quantum efficiency (EQE) value using the relation (5) [36] and shown in Table 2.

$$\text{EQE} = R\frac{hc}{e\lambda}. \tag{5}$$

Here all symbols are in usual meaning. The calculated EQE value lies in the order 140% > 76% > 47% for 0.1, 0.15, 0.15 M, respectively. Shkir and his lab mates [37] reached EQE value up to 143% for Eu-implanted CdS thin films. Mianzeng Zhong et al. [66] prepared samples to exhibit a maximum efficiency of 4.07×10^4%.

To estimate the rise and fall time, photoresponse switching performance was done with five different powers (from 1 to 5 mW/cm^2). Figure 8a–c elaborates on the sequential switching performance of photoresponse. When the laser light falls on the CdS thin film the photocurrent is quickly increased and reaching a saturation level and further it is decreased when the laser is turned off. Here the photocurrent of the 0.1 M deposited product

Table 2 Critical parameters of currently fabricated CdS thin film photodetectors and earlier reports on CdS-nanostructure photodetectors

Device	Spectral range	R (AW^{-1})	EQE (%)	D^* (Jones)	Photoresponse (I_{light}/I_{dark})	Rise time τ_{rise}	Fall time τ_{fall}	References
0.05 M CdS	532 nm	0.15	47	3.48×10^{10}	–	0.3	0.5	Current work
0.10 M CdS		0.43	140	8.46×10^{10}	–	0.2	0.3	
0.15 M CdS		0.24	76	5.10×10^{10}	–	0.3	0.4	
Pure CdS	532 nm	0.213	49.70	7.43×10^{11}	2×10^3	138 ms	120 ms	[36]
0.1% Sm:CdS		1.101	257	2.21×10^{12}	4.9×10^3	157 ms	166 ms	
CdS:Ga (2%) NR/Au	510 nm	4	–	–	12×10^3	95 µs	290 µs	[13]
CdS NB MESFET	488 nm	2.0×10^2	529	–	2.7×10^6	137 µs	379 µs	[16]
CdS:Ag heterojunction	551 nm	0.43	91.42	2.58×10^{11}	–	–	–	[68]
CdS hierarchical NWs	470 nm	–	–	4.27×10^{12}	1.96×10^4	0.3 s	0.4 s	[18]
CdS NT	532 nm	–	–	–	4.02×10^3	0.82 s	0.63 s	[67]
CdS NWs		–	–	–	7.41×10^2	0.4 s	0.7	
CdS NB	490 nm	7.3×10^4	1.9×10^7	–	6	20 µs	20 µs	[17]
5 wt.% Pr:CdS	532 nm	2.71	628.86	6.94×10^{11}	3.95×10^2	0.090 s	0.170 s	[69]
5 wt.% Eu:CdS	532 nm	0.614	143	1.38×10^{12}	4.3×10^3	85 ms	106 ms	[70]
CdS NPs	420 nm	0.38	–	2.6×10^{13}	207	–	–	[65]
CdS NPs	500-nm	0.24	–	–	97.2×10^3	9 ms	10 ms	[66]
CdS NPs	Visible	–	–	–	1123	25 ms	25 ms	[67]
CdS:Ag	551 nm	0.43	–	2.58×10^{11}	–	–	–	[17]

NWs nanowires, *NB* nanobelt, *NR* nanorods, *NT* nanotubes, *NPs* nanoparticles

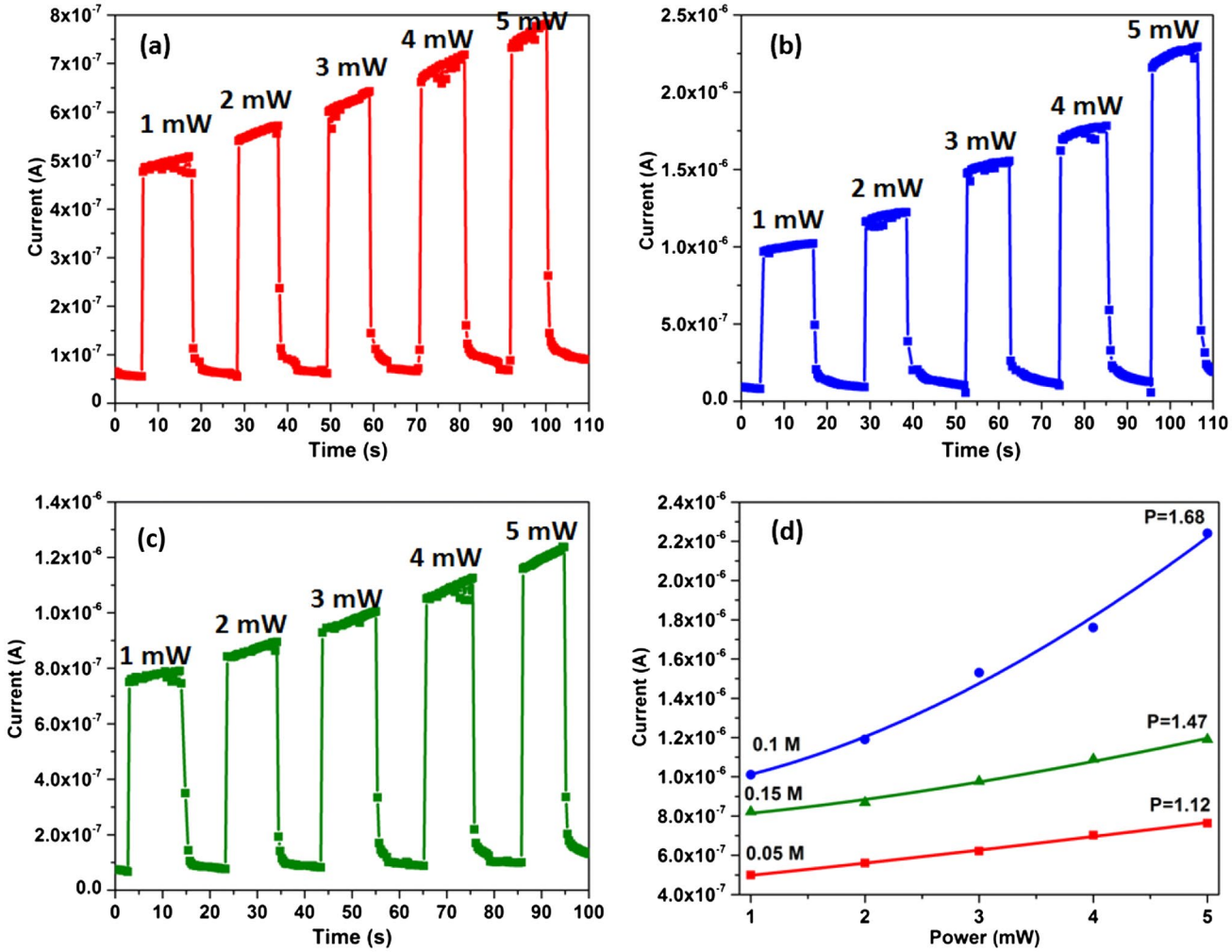

Fig. 8 Plots of current vs. time of CdS thin films at different molar concentrations **a** 0.05 M, **b** 0.10 M, **c** 0.15 M and **d** a plot of fitted (solid line) photocurrent as a function of illumination intensity of CdS thin films at different molar concentrations

is changed from 7.518×10^{-8} to 2.474×10^{-6} A as the light is ON state at a voltage of 5 V (bias). The rise and fall time were computed for all photodetector samples. The rise time of CdS thin films is 0.3, 0.2, 0.3 s, and fall times are 0.5, 0.3, and 0.4 s for the films prepared by 0.05, 0.1, and 0.15 M, respectively (see Table 2). Here the 0.1 M fabricated sample deposited onto the glass slide shows fast response and recovery times of 0.2 s and 0.3 s. Ludong Li et al. [18] reported rise and fall times were about 0.3 and 0.4 s. CdS nanotubes synthesized by Qinwei An et al. [67] shows the rise and fall times of 0.82 s and 0.63 s. However, Liang Li et al. [17] reduced the raise time up to 20 µs for CdS nanobelts. For better comparison, the output results of current, as well as several previously reported photodetectors are listed in Table 2, which indicates the fabricated detectors are far better than reported by several others based on CdS. Figure 8d proves the photogenerated current reliance on the intensity of light of the manufactured samples. Here, symbol and experimental results represented by the solid line and curve fitted by [36]

$$I_{\mathrm{ph}} = \alpha \phi^{n}, \tag{6}$$

where α, n, are constant and empirical exponent to illuminating strength. Photodetection nature and recombination progression in the device can be conferred via n value. By polynomial fitting of experimental data, n values are noticed from graphs and its value is nearly the same for all films. So, we are only displaying a graph at 5 V. The maximum n value is noted ~ 1.68 for 0.1 M CdS film. It reveals that the film prepared with a molar concentration of 0.1 M excellently diminishes the trap of CdS films, as a result, produces better performable CdS photodetectors equated to film prepared with other molar concentrations.

4 Conclusions

In this work, molarities of cationic and anionic precursors are varied simultaneously for depositing the CdS films and their structural, optoelectronic properties are analyzed in detail. The grown films possess the hexagonal crystal system with preferential (002) direction of growth. The enlarged grain size with uniform morphology, obtained at 0.1 M precursor molar concentration. Bandgap value was altered as 2.39 and 2.43 eV by controlling the precursor molarity 0.05 and 0.15 M. The thin film prepared at 0.10 M is having good photodetector properties compare to others due to the improved crystallinity and surface morphology. These outcomes are attained without further processing of films. Hence, they are fairly advantageous for developing cost-effective CdS film-based photodetectors of visible light with fast response, detectivity, and efficiency.

Acknowledgements The authors extend their sincere appreciation to the Deanship of Scientific Research at Princess Nourah bint Abdulrahman University for funding this research through the Fast-track Research Funding Program.

Compliance with ethical standards

Conflict of interest There are no conflicts to declare.

References

1. R. Vrijen, E. Yablonovitch, A spin-coherent semiconductor photodetector for quantum communication. Phys. E **10**(4), 569–575 (2001)
2. R. Hattori, M. Hironaka, Semiconductor photodetector device, Google Patents, (1991).
3. P.H. Shen, M.R. Stead, M.A. Taysing-Lara, J. Pamulapati, W.C. Ruff, B.L. Stann, P.N. Uppal, *Interdigitated Finger Semiconductor Photodetector for Optoelectronic Mixing, Infrared Detectors and Focal Plane Arrays VI* (International Society for Optics and Photonics, Bellingham, 2000), pp. 426–435
4. M. Tsuji, Ultraspeed low-voltage drive avalanche multiplication type semiconductor photodetector, Google Patents (2002).
5. Z. Qi, T. Yang, D. Li, H. Li, X. Wang, X. Zhang, F. Li, W. Zheng, P. Fan, X. Zhuang, A. Pan, High-responsivity two-dimensional p-PbI2/n-WS2 vertical heterostructure photodetectors enhanced by photogating effect. Materials Horizons **6**, 1474–1480 (2019)
6. F. Xia, T. Mueller, Y.-M. Lin, A. Valdes-Garcia, P. Avouris, Ultrafast graphene photodetector. Nat. Nanotechnol. **4**(12), 839 (2009)
7. S. Najmaei, M. Dubey, 2d material photo-detector gain and responsivity control and enhancement through induced interface trap doping, Google Patents, (2019).
8. P. Gant, P. Huang, D.P. de Lara, D. Guo, R. Frisenda, A. Castellanos-Gomez, A strain tunable single-layer MoS2 photodetector. Mater. Today **27**, 8–13 (2019)
9. S. Edwards, T. Oder, *Characterization of Ultraviolet ZnO Photodetector* (Bulletin of the American Physical Society, Boston, 2019)
10. M. Long, Y. Wang, P. Wang, X. Zhou, H. Xia, C. Luo, S. Huang, G. Zhang, H. Yan, Z. Fan, X. Wu, X. Chen, W. Lu, W. Hu, Palladium diselenide long-wavelength infrared photodetector with high sensitivity and stability. ACS Nano **13**(2), 2511–2519 (2019)
11. L.H. Zeng, D. Wu, S.H. Lin, C. Xie, H.Y. Yuan, W. Lu, S.P. Lau, Y. Chai, L.B. Luo, Z.J. Li, Controlled synthesis of 2D palladium diselenide for sensitive photodetector applications. Adv. Func. Mater. **29**(1), 1806878 (2019)
12. F. Cao, L. Meng, M. Wang, W. Tian, L. Li, Gradient energy band driven high-performance self-powered perovskite/CdS photodetector. Adv. Mater. **31**(12), 1806725 (2019)
13. D. Wu, Y. Jiang, Y. Zhang, Y. Yu, Z. Zhu, X. Lan, F. Li, C. Wu, L. Wang, L. Luo, Self-powered and fast-speed photodetectors based on CdS: Ga nanoribbon/Au Schottky diodes. J. Mater. Chem. **22**(43), 23272–23276 (2012)
14. M. Shuai, Y. Lingmin, C. Lei, L. Chun, Y. Mingli, F. Xinhui, Resistive-type UV–visible photodetector based on CdS NWs / ZnO nanowalls heterostructure fabricated using in-situ synthesis method. J. Alloy. Compd. **827**, 154090 (2020)
15. K. Deng, L. Li, CdS Nanoscale Photodetectors. Adv. Mater. **26**(17), 2619–2635 (2014)
16. Y. Ye, L. Dai, X. Wen, P. Wu, R. Pen, G. Qin, High-Performance Single CdS Nanobelt Metal-Semiconductor Field-Effect Transistor-Based Photodetectors. ACS Appl. Mater. Interfaces. **2**(10), 2724–2727 (2010)
17. L. Li, P. Wu, X. Fang, T. Zhai, L. Dai, M. Liao, Y. Koide, H. Wang, Y. Bando, D. Golberg, Single-crystalline CdS nanobelts for excellent field-emitters and ultrahigh quantum-efficiency photodetectors. Adv. Mater. **22**(29), 3161–3165 (2010)
18. L. Li, Z. Lou, G. Shen, Hierarchical CdS Nanowires Based Rigid and Flexible Photodetectors with Ultrahigh Sensitivity. ACS Appl. Mater. Interfaces. **7**(42), 23507–23514 (2015)
19. M. Mahdi, J. Hassan, S. Ng, Z. Hassan, N.M. Ahmed, Synthesis and characterization of single-crystal CdS nanosheet for high-speed photodetection. Phys. E **44**(7–8), 1716–1721 (2012)
20. J. Jie, W. Zhang, Y. Jiang, X. Meng, Y. Li, S. Lee, Photoconductive characteristics of single-crystal CdS nanoribbons. Nano Lett. **6**(9), 1887–1892 (2006)
21. Z. Lou, L. Li, G. Shen, Ultraviolet/visible photodetectors with ultrafast, high photosensitivity based on 1D ZnS/CdS heterostructures. Nanoscale **8**(9), 5219–5225 (2016)
22. L. Zhu, C. Li, Y. Li, C. Feng, F. Li, D. Zhang, Z. Chen, S. Wen, S. Ruan, Visible-light photodetector with enhanced performance based on a ZnO@ CdS heterostructure. J. Mater. Chem. C **3**(10), 2231–2236 (2015)
23. X.-X. Yu, H. Yin, H.-X. Li, W. Zhang, H. Zhao, C. Li, M.-Q. Zhu, Piezo-phototronic effect modulated self-powered UV/visible/near-infrared photodetectors based on CdS: P3HT microwires. Nano Energy **34**, 155–163 (2017)
24. B. Mereu, G. Sarau, E. Pentia, V. Draghici, M. Lisca, T. Botila, L. Pintilie, Field-effect transistor based on nanometric thin CdS films. Mater. Sci. Eng., B **109**(1–3), 260–263 (2004)
25. R. Ma, L. Dai, G. Qin, Enhancement-mode metal-semiconductor field-effect transistors based on single n-Cd S nanowires. Appl. Phys. Lett. **90**(9), 093109 (2007)
26. Z. Qian, H.-J. Bai, G.-L. Wang, J.-J. Xu, H.-Y. Chen, A photoelectrochemical sensor based on CdS-polyamidoamine nano-composite film for cell capture and detection. Biosens. Bioelectron. **25**(9), 2045–2050 (2010)
27. L. Yadava, R. Verma, R. Dwivedi, Sensing properties of CdS-doped tin oxide thick film gas sensor. Sens. Actuators B Chem. **144**(1), 37–42 (2010)
28. Y.L. Lee, Y.S. Lo, Highly efficient quantum-dot-sensitized solar cell based on co-sensitization of CdS/CdSe. Adv. Func. Mater. **19**(4), 604–609 (2009)

29. S. Bhushan, D. Thakur, Photoconductivity of chemically deposited rare-earth-doped CdS films. J. Mater. Sci. Mater. Electron. **3**(1), 35–40 (1992)
30. M.A. Mahdi, J.J. Hassan, N.M. Ahmed, S.S. Ng, Z. Hassan, Growth and characterization of CdS single-crystalline microrod photodetector. Superlattices Microstruct. **54**, 137–145 (2013)
31. D. Wu, Y. Jiang, S. Li, F. Li, J. Li, X. Lan, Y. Zhang, C. Wu, L. Luo, J. Jie, Construction of high-quality CdS: Ga nanoribbon/silicon heterojunctions and their nano-optoelectronic applications. Nanotechnology **22**(40), 405201 (2011)
32. M. Husham, Z. Hassan, A.M. Selman, N.K. Allam, Microwave-assisted chemical bath deposition of nanocrystalline CdS thin films with superior photodetection characteristics. Sens. Actuators A **230**, 9–16 (2015)
33. M. Waldiya, R. Narasimman, D. Bhagat, D. Vankhade, I. Mukhopadhyay, Nanoparticulate CdS 2D array by chemical bath deposition: Characterization and optoelectronic study. Mater. Chem. Phys. **226**, 26–33 (2019)
34. S. Munde, N. Shinde, P. Khanzode, M. Budrukkar, P. Lahane, J. Dadge, S. Jejurikar, M. Mahabole, R. Khairnar, K. Bogle, Nanocrystalline CdS thick films: a highly sensitive photo-detector. Mater. Res. Express **5**(6), 066203 (2018)
35. M. Shkir, I. Ashraf, S. AlFaify, A.M. El-Toni, M. Ahmed, A. Khan, A noticeable effect of Pr doping on key optoelectrical properties of CdS thin films prepared using spray pyrolysis technique for high-performance photodetector applications. Ceram. Int. **46**(4), 4652–4663 (2020)
36. M. Shkir, I. Ashraf, A. Khan, M.T. Khan, A.M. El-Toni, S. AlFaify, A facile spray pyrolysis fabrication of Sm: CdS thin films for high-performance photodetector applications. Sens. Actuators A **306**, 111952 (2020)
37. M. Shkir, I.M. Ashraf, K.V. Chandekar, I.S. Yahia, A. Khan, H. Algarni, S. AlFaify, A significant enhancement in visible-light photodetection properties of chemical spray pyrolysis fabricated CdS thin films by novel Eu doping concentrations. Sens. Actuators A **301**, 111749 (2020)
38. L. Wenyi, C. Xun, C. Qiulong, Z. Zhibin, Influence of growth process on the structural, optical and electrical properties of CBD-CdS films. Mater. Lett. **59**(1), 1–5 (2005)
39. F. Atay, V. Bilgin, I. Akyuz, S. Kose, The effect of In doping on some physical properties of CdS films. Mater. Sci. Semicond. Process. **6**(4), 197–203 (2003)
40. P.J. Sebastian, p-type CdS thin films formed by in situ Cu doping in the chemical bath. Appl. Phys. Lett. **62**(23), 2956–2958 (1993)
41. R. Bairy, A. Jayarama, G.K. Shivakumar, S.D. Kulkarni, S.R. Maidur, P.S. Patil, Effect of Aluminium doping on photoluminescence and third-order nonlinear optical properties of nanostructured CdS thin films for photonic device applications. Phys. B **555**, 145–151 (2019)
42. L.A. González, I. Carreón-Moncada, M.A. Quevedo-López, Negative differential resistance as effect of Zn doping of chemically processed CdS thin film transistors. Mater. Lett. **192**, 161–164 (2017)
43. M. Paulraj, S. Ramkumar, K.P. Varkey, K.P. Vijayakumar, C. Sudha Kartha, K.G.M. Nair, Characterizations of undoped and Cu doped CdS thin films using photothermal and other techniques. Phys. Status Solidi (a) **202**(3), 425–434 (2005)
44. S. Chander, M.S. Dhaka, Optical and structural constants of CdS thin films grown by electron beam vacuum evaporation for solar cells. Thin Solid Films **638**, 179–188 (2017)
45. M. Shkir, M. Anis, S. Shafik, M.A. Manthrammel, M.A. Sayeed, M.S. Hamdy, S. AlFaify, An effect of Zn content doping on upto-third order nonlinear characteristics of nanostructured CdS thin films fabricated through spray pyrolysis for optoelectronics. Phys. E **118**, 113955 (2020)
46. P. Parameshwari, K.G. Naik, *Effect of Cd/S Molar Ratio on the Optical and Electrical Properties of Spray Deposited CdS Thin Films, Physics of Semiconductor Devices* (Springer, Berlin, 2014), pp. 347–349
47. S. Yılmaz, Y. Atasoy, M. Tomakin, E. Bacaksız, Comparative studies of CdS, CdS:Al, CdS: Na and CdS:(Al–Na) thin films prepared by spray pyrolysis. Superlattices Microstruct. **88**, 299–307 (2015)
48. V. Senthamilselvi, K. Saravanakumar, N.J. Begum, R. Anandhi, A. Ravichandran, B. Sakthivel, K. Ravichandran, Photovoltaic properties of nanocrystalline CdS films deposited by SILAR and CBD techniques—a comparative study. J. Mater. Sci. Mater. Electron. **23**(1), 302–308 (2012)
49. K. Ravichandran, P. Philominathan, Investigations on microstructural and optical properties of CdS films fabricated by a low-cost, simplified spray technique using perfume atomizer for solar cell applications. Sol. Energy **82**(11), 1062–1066 (2008)
50. S. Gosavi, C. Nikam, A. Shelke, A. Patil, S.-W. Ryu, J. Bhat, N. Deshpande, Chemical synthesis of porous web-structured CdS thin films for photosensor applications. Mater. Chem. Phys. **160**, 244–250 (2015)
51. A.A. Ziabari, F. Ghodsi, Effects of the Cd: Zn: S molar ratio and heat treatment on the optical and photoluminescence properties of nanocrystalline CdZnS thin films. Mater. Sci. Semicond. Process. **16**(6), 1629–1636 (2013)
52. K.A. Aly, N. Khalil, Y. Algamal, Q.M. Saleem, Lattice strain estimation for CoAl2O4 nano particles using Williamson-Hall analysis. J. Alloy. Compd. **676**, 606–612 (2016)
53. N. Anitha, M. Anitha, J. Raj Mohamed, S. Valanarasu, L. Amalraj, Influence of tin precursor concentration on physical properties of nebulized spray deposited tin disulfide thin films. J. Asian Ceram. Soc. **6**(2), 121–131 (2018)
54. S. AlFaify, L. Haritha, M.A. Manthrammel, V. Ganesh, K.V. Chandekar, S.S. Shaikh, M. Shkir, Fabrication and characterization of Sn:CdS films for optical-nonlinear-limiting applications. Opt. Laser Technol. **126**, 106122 (2020)
55. H. Kumar, S. Kumar, Indium sulfide based metal-semiconductor-metal ultraviolet-visible photodetector. Sens. Actuators A **299**, 111643 (2019)
56. M.S. Mahdi, K. Ibrahim, A. Hmood, N.M. Ahmed, S.A. Azzez, F.I. Mustafa, A highly sensitive flexible SnS thin film photodetector in the ultraviolet to near infrared prepared by chemical bath deposition. RSC Adv. **6**(116), 114980–114988 (2016)
57. M. Husham, Z. Hassan, M. Mahdi, A.M. Selman, N.M. Ahmed, Fabrication and characterization of nanocrystalline CdS thin film-based optical sensor grown via microwave-assisted chemical bath deposition. Superlattices Microstruct. **67**, 8–16 (2014)
58. K. Wilson, M.B. Ahamed, Influence of bath temperature on surface modification and optoelectronic properties of chemical bath deposited CdS thin film nanostructures. Mater. Sci. Eng. B **251**, 114444 (2019)
59. N. Saxena, T. Kalsi, P. Uttam, P. Kumar, Morphological evolution in nanocrystalline CdS thin films from flowers to salt rock like structures. Opt. Mater. **84**, 625–630 (2018)
60. R. Khalfi, D. Talantikite-Touati, A. Tounsi, H. Merzouk, Effect of deposition time on structural and optical properties of ZnSe thin films grown by CBD method. Opt. Mater. **106**, 109989 (2020)
61. T.S. Reddy, M.S. Kumar, Co-evaporated SnS thin films for visible light photodetector applications. RSC Adv. **6**(98), 95680–95692 (2016)
62. M. Nair, P. Nair, Simplified chemical deposition technique for good quality SnS thin films. Semicond. Sci. Technol. **6**(2), 132 (1991)
63. M. Shkir, Z.R. Khan, M. Anis, S.S. Shaikh, S. AlFaify, A comprehensive study of opto-electrical and nonlinear properties of Cu@CdS thin films for optoelectronics. Chin. J. Phys. **63**, 51–62 (2020)

64. M. Husham, Z. Hassan, A.M. Selman, Synthesis and characterization of nanocrystalline CdS thin films for highly photosensitive self-powered photodetector. Eur. Phys. J. Appl. Phys. **74**(1), 10101 (2016)
65. M. Tan, C. Hu, Y. Lan, J. Khan, H. Deng, X. Yang, P. Wang, X. Yu, J. Lai, H. Song, 2D lead dihalides for high-performance ultraviolet photodetectors and their detection mechanism investigation. Small **13**(47), 1702024 (2017)
66. M. Zhong, L. Huang, H.-X. Deng, X. Wang, B. Li, Z. Wei, J. Li, Flexible photodetectors based on phase dependent PbI 2 single crystals. J. Mater. Chem. C **4**(27), 6492–6499 (2016)
67. Q. An, X. Meng, P. Sun, High-performance fully nanostructured photodetector with single-crystalline CdS Nanotubes as active layer and very long ag nanowires as transparent electrodes. ACS Appl. Mater. Interfaces. **7**(41), 22941–22952 (2015)
68. N.I. Najm, H.K. Hassun, B. KH al-Maiyaly, B.H. Hussein, A.H. Shaban, Highly selective CdS: Ag heterojunction for photodetector applications, in AIP Conference Proceedings, AIP Publishing (2019), p. 020031.
69. M. Shkir, I.M. Ashraf, S. AlFaify, A.M. El-Toni, M. Ahmed, A. Khan, A noticeable effect of Pr doping on key optoelectrical properties of CdS thin films prepared using spray pyrolysis technique for high-performance photodetector applications. Ceram. Int. **46**, 4652–4653 (2019)
70. M. Shkir, I.M. Ashraf, K.V. Chandekar, I.S. Yahia, A. Khan, H. Algarni, S. AlFaify, A significant enhancement in visible-light photodetection properties of chemical spray pyrolysis fabricated CdS thin films by novel Eu doping concentrations. Sens. Actuators A Phys. **111749**, 301 (2019)